Influence of trapped and interfacial charges in organic multilayer lightemitting devices

by W. Riess H. Riel T. Beierlein W. Brütting P. Müller

P. F. Seidler

Trapped and interfacial charges have significant impact on the performance of organic light-emitting devices (OLEDs). We have studied devices consisting of 20 nm copper phthalocyanine (CuPc) as the buffer and hole-injection layer, 50 nm N,N'di(naphthalene-1-yl)-N,N'-diphenyl-benzidine (NPB) as the hole transport layer, and 65 nm tris(8-hydroxyquinolinato)aluminum (Alq₃) as the electron transport and emitting layer sandwiched between a high-work-function metal and a semitransparent Ca electrode. Current-voltage measurements show that the device characteristics in the negative bias direction and at low positive bias below the built-in voltage are influenced by trapped charges within the organic layers. This is manifested by a strong dependence of the current in this range on the direction and speed of the voltage sweep. Low-frequency capacitance-voltage and static charge

measurements reveal a voltage-independent capacitance in the negative bias direction and a significant increase between 0 and 2 V in the given device configuration, indicating the presence of negative interfacial charges at the NPB/Alq₃ interface. Transient experiments show that the delay time of electroluminescence at low voltages in these multilayer devices is controlled by the buildup of internal space charges, which facilitates electron injection, rather than by chargecarrier transport through the organic layers. To summarize, our results clearly demonstrate that the tailoring of internal barriers in multilayer devices leads to a significant improvement in device performance.

1. Introduction

Early work on molecular crystals clearly demonstrated that the relevant mechanism of electroluminescence (EL) in

©Copyright 2001 by International Business Machines Corporation. Copying in printed form for private use is permitted without payment of royalty provided that (1) each reproduction is done without alteration and (2) the *Journal* reference and IBM copyright notice are included on the first page. The title and abstract, but no other portions, of this paper may be copied or distributed royalty free without further permission by computer-based and other information-service systems. Permission to *republish* any other portion of this paper must be obtained from the Editor.

0018-8646/01/\$5.00 © 2001 IBM



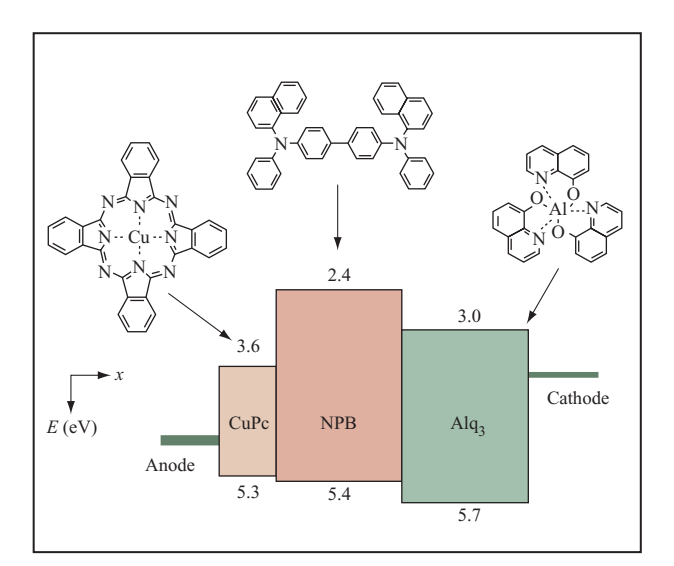


Figure 1

Schematic energy-level diagram and chemical structures of the organic materials used for the OLEDs.

organic solids is of the injection type [1]. Injection luminescence requires several steps, including the injection, transport, capture, and radiative recombination of positive and negative charge carriers inside an organic layer with an energy gap suitable for yielding visible light output. A very successful approach to separately optimizing these individual steps is the concept of organic multilayer light-emitting devices (LEDs) using heterointerfaces between different organic materials [2]. The simplest organic LED (OLED) of this kind incorporates a hetero-interface between a hole-conducting material (usually a triphenyl-amine derivative) and an electron-conducting aluminum chelate complex (Alq₃), where light emission is generated in the Alq₃ layer close to the organic–organic interface [3].

The optimization of these devices requires on the one hand an improvement in the fluorescence yield of the emitting material, which can be achieved by doping, and on the other hand a well-balanced injection of positive and negative charge carriers. Moreover, since these devices are current-driven, good charge-carrier-transport capabilities are considered a prerequisite for a high luminous efficiency. For example, low charge-carrier mobilities ($\mu \ll 1 \text{ cm}^2/\text{Vs}$) can lead to space-charge-limited currents, especially if one contact is able to inject more carriers than would be present in thermal equilibrium [4], and thus limit the device performance [5–8]. Furthermore, in the presence of an organic–organic interface in a hetero- or multilayer device, the energy level offset at the interface can be an additional source of the

buildup of interfacial space charges. Even in the absence of these energy barriers, the abrupt differences of charge-carrier mobilities in the respective layers of typical multilayer devices (see Section 4) lead in effect to the presence of mobility barriers at hetero-interfaces, which in turn can be the source of interfacial space-charge formation. Obviously, knowledge of the charge and field distributions inside a device as well as their variation with the applied voltage is crucial for the physical understanding of device operation. Also, from the viewpoint of technical applications, the avoidance of space charge is important for device optimization with respect to efficiency, temporal response, and long-term stability.

In the following sections we describe our experimental evidence for the presence of space charges in metal anode/CuPc/NPB/Alq₃/Ca devices by current–voltage, capacitance–voltage, and transient electroluminescence measurements.

2. Device preparation and experimental methods

Our devices are built on glass substrates (Schott AF 45) precoated with a high-work-function anode such as ITO, Pt, Ir, Ni, or Pd (≈75 nm thick). The organic multilayer structure consists of CuPc as the buffer layer, NPB as the hole transport layer, and Alq, as the electron-transporting and emitting layer (Figure 1). The thicknesses of the different organic layers are given in the body of the paper. When a metal anode was used, EL was observed through a 20-nmthick Ca cathode. The active area of each of our devices was 2 mm × 3 mm. Prior to use, all organic materials were purified by vacuum sublimation. Depositions were carried out in a high-vacuum system (Leybold) by thermal evaporation from resistively heated tantalum and tungsten boats. The base pressure in the chamber ranged between 4×10^{-7} and 1×10^{-6} mbar. Typical deposition rates for the organic compounds and the metal were 1 Å/s. The evaporation chamber is attached directly to an argon glove-box system, which allows devices to be fabricated, characterized, and encapsulated under inert conditions. Current-voltage (I-V) and luminance-voltage (EL-V)characteristics were measured with a Hewlett-Packard parameter analyzer (HP 4145B) and a sensitive Si photodiode (Hamamatsu S2281). The luminance calibration of the photodiode was obtained with a Photo Research PR704 spectroradiometer. Transient electroluminescence (TEL) was measured in a specially designed setup that allows one to detect simultaneously time-dependent EL, current, and voltage across the device. The OLEDs were characterized in a modified HP 16058A test fixture with a Hamamatsu photomultiplier 5783-01 (time resolution ≈ 0.65 ns) located directly on top of the emitting area to detect EL intensity. An HP 8116A dc pulse/function generator (50 MHz, rise time ≈ 7 ns, decay

time ≈ 10 ns) was used to apply rectangular voltage pulses to the device. The pulse length was varied between 8 and 300 ms, with a duty cycle of 10%. The function generator permits the OLED to be driven with various positive and negative offset voltages before the rectangular voltage pulses are applied. The photomultiplier was connected to the $50-\Omega$ input resistance of a digital oscilloscope (Tektronix 2440) to record the EL signal. A second digital oscilloscope (Tektronix 2440) allowed one to monitor the voltage pulse and the time-dependent current flow through the device simultaneously with the EL signal. Impedance (Z) and capacitance-voltage (C-V) measurements were carried out with a frequency response analyzer (Solartron Instruments SI1260). Typically the oscillator level was set to 50 mV, and the measurement was averaged over 100 cycles of the respective frequencies. Static discharge measurements were performed with a Keithley electrometer (EM 617) and the device affixed in an HP 8116A test fixture. Charging of the OLED was performed for a distinct time of one minute by the built-in voltage source of the electrometer. Directly after charging, the device was separated from the source and connected to the Coulomb input of the electrometer to measure the total stored charge of the OLED. Switching was done manually, and because of the excellent electrical isolation of the setup and the high impedance of the device, discharging effects became negligible at low voltages. All measurements were carried out with encapsulated devices at room temperature.

3. Experimental results

Current-voltage characteristics

Figure 2 shows the dependence of I-V and EL-Vcharacteristics on sweep direction and sweep speed for a metal anode/CuPc/NPB/Alq₃/Ca device. In Figure 2(a) the voltage has been incremented in steps of 50 mV from −3 to 7 V and back again. Current and brightness were detected with the parameter analyzer set to a "medium" integration time¹ and the delay time between individual data points to 0. In this mode, the time required for acquisition of a single data point depends on the magnitude of the detected current and ranges from 10 to 100 ms for the given device. Figure 2(b) was measured with a "long" integration time and an additional delay of 10 s between individual data points. In both cases the current increases strongly in the forward bias direction above a threshold voltage of 2 V and is virtually unaffected by sweep direction and speed. The onset of EL determined at 0.1 mcd/m² is 2.1 V. This onset is not

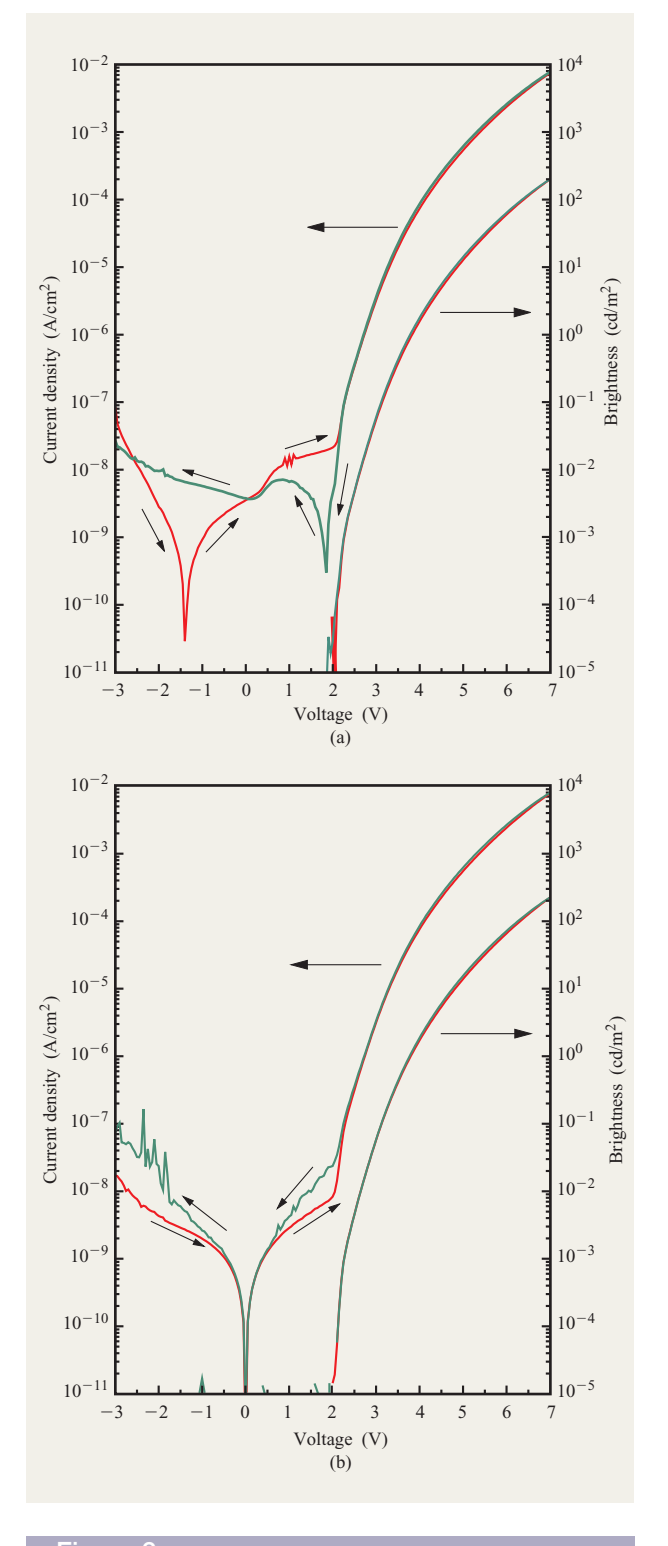


Figure 2

Current–voltage and brightness–voltage characteristics of an anode/ CuPc (20 nm)/NPB (50 nm)/ Alq $_3$ (65 nm)/Ca device measured in different sweep directions and with different delay and integration times between individual voltage steps: (a) "medium" integration time and 0 s delay time; (b) "long" integration time and 10 s delay time. From [9].

¹ It is difficult to give an accurate definition of a "medium," "long," or "fast" time, since the actual time depends not only on the integration time but also on the current range. Therefore, the total time depends on the impedance of the device structure and the integration time (see HP Manual 4145B).



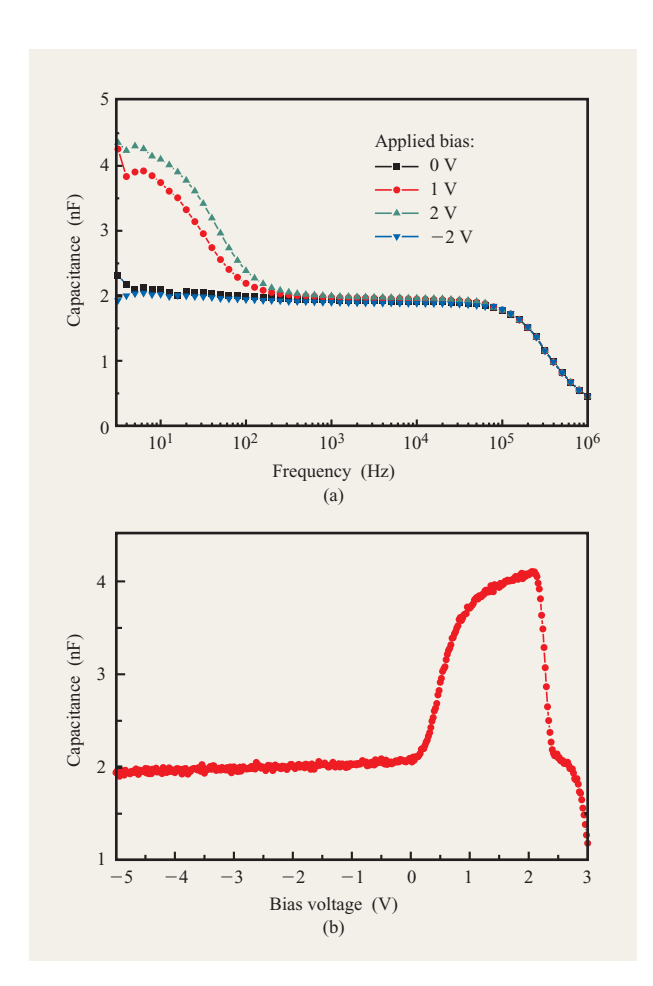


Figure 3

Dependence of the capacitance on (a) frequency and (b) applied bias of the same device at 10 Hz as in Figure 2. Adapted from [9].

affected by external parameters. We note that the onset voltage for detectable EL is significantly lower than the optical gap of Alq₃ (2.7 eV) and rather corresponds to the built-in voltage (i.e., difference in work function) of the two electrodes. Remarkable differences in the current flow are observed below 2 V, where no detectable EL and thus no double carrier injection takes place. The measurement with integration time "medium" shows a strong hysteresis between up and down sweeps [Figure 2(a)]. In particular, the voltage at which the current passes through zero is not at zero bias but at about -1.4 V for increasing voltage and around +1.9 V for the other sweep direction. Furthermore, under these measurement conditions a steplike structure at about 0.5 V is observed in both sweep directions, which we found to be characteristic for a multilayer structure containing CuPc. We do not observe this feature if the CuPc layer is omitted. The delay time of 10 s between subsequent data points used in the slow

measurement is sufficient to achieve zero crossing of the current at 0 V. In addition, the structure at about 0.5 V disappears. The described hysteresis of the I-V characteristics is a clear indication of the presence of space charges in the device. During these measurements we observe a higher current for decreasing voltage between 2 and 0.5 V and below -1 V. In these regimes the current is also relatively noisy. This is most likely caused by leakage currents, which can occur after the device has been operated for longer times at higher positive bias. However, these leakage currents are reversible and can be suppressed by applying negative voltage for a certain time.

Bias-dependent capacitance

The measurement of bias- and frequency-dependent device capacitance is a well-established technique for the investigation of conductivity, doping concentration, and trap states/density in organic semiconductors. For some polymeric semiconductors, this method has been successfully used to prove the existence of p-type doping leading to Schottky junctions with low-work-function metals [10–12]. Furthermore, in combination with temperature-dependent measurements, the energy of shallow acceptor states and deep trap states has been determined [13]. The materials used in this study, especially NPB and Alq,, are expected to have very few intrinsic carriers and extrinsic dopants. In addition, they have been purified before usage. Only CuPc is known to be easily doped by atmospheric oxygen, leading to p-type conducting behavior [14, 15]. Thus, in the absence of free or trapped charges inside the device, we expect to measure a bias- and frequency-independent device capacitance corresponding to a series of three dielectric media with dielectric constants $\varepsilon_{r,i}$, thickness d_i , and area A. Given the active device area and thickness of the individual layers together with the dielectric constants of the materials in the range of 3.5 to 4, one can estimate the device capacitance to be about 1.5 to 2 nF.

Figure 3 shows the capacitance as a function of frequency of the same device as in Figure 2 for different applied bias values and as a function of bias for a fixed frequency of 10 Hz. The frequency-dependent measurements in Figure 3(a) show that at zero and negative bias the capacitance is essentially frequency-independent up to some 10^4 Hz, with a value in the neighborhood of 2 nF, as estimated above. Above 10^5 Hz the capacitance drops rapidly to a value much lower than the one corresponding to the dielectric constants of the materials. This can be ascribed to parasitic effects due to lead/contact resistances and capacitances, which are not discussed further here. The frequency dependence of the capacitance is almost identical for all applied bias values above ≈ 200 Hz. Below 200 Hz and for positive bias

(1 and 2 V), an increase in the capacitance is observed. At low frequencies (f < 10 Hz), the capacitance seems to saturate at a value independent of the bias. To study the bias dependence in more detail, the applied bias was varied at a fixed frequency of 10 Hz. This frequency is in most cases low enough to monitor the saturation value of the capacitance at low frequencies and still gives a good signal-to-noise ratio. The curves shown in Figure 3(b) were taken from -5 to 3 V in steps of 25 mV, with an additional delay of 10 s between the individual data points. No difference was observed for the opposite sweep direction. Whereas there is only a very weak bias dependence in the negative direction, the capacitance increases significantly for positive bias at about 0.2 V and reaches a maximum at 2.1 V, which coincides with the onset of EL. Above this voltage the capacitance decreases sharply to a value of about 2 nF before it finally drops further as the bias exceeds 2.5 V. It is important to note that in the regime of double carrier injection accompanied by recombination, the capacitance is not well defined; thus, no measurements for voltages above 3 V have been performed.

To determine the low-frequency saturation value of the device capacitance, we have performed static discharge measurements. Figure 4 shows the measured charge Q for different charging voltages V and the calculated capacitance using the relation

$$C = \frac{\Delta Q}{\Delta V}.\tag{1}$$

Although the scattering of data is considerable, it is clear that the capacitance in the positive bias direction increases and reaches a maximum at 2 V with a value about twice as high as in the negative direction. At 2 V, the maximum value of 5 nF is slightly higher than that obtained in frequency-dependent measurements, indicating that in the latter the capacitance has not reached its saturation value at the frequency of 10 Hz used here. In the negative bias direction, the capacitance has approximately the same constant value of 2 nF as in the ac measurement. The slight decrease for increasing negative bias can be explained as a consequence of leakage currents leading to a partial discharge during the time of switching between the voltage source and the Coulomb meter. Consequently, the measuring error increases with higher negative voltage.

Transient electroluminescence (TEL)

In TEL measurements one is interested in the timeresolved EL response to a pulse excitation, usually a rectangular voltage pulse. **Figure 5** shows typical current and EL signals upon excitation with a rectangular voltage pulse (4 V). The EL signal is characterized by a finite delay time between the application of the voltage pulse

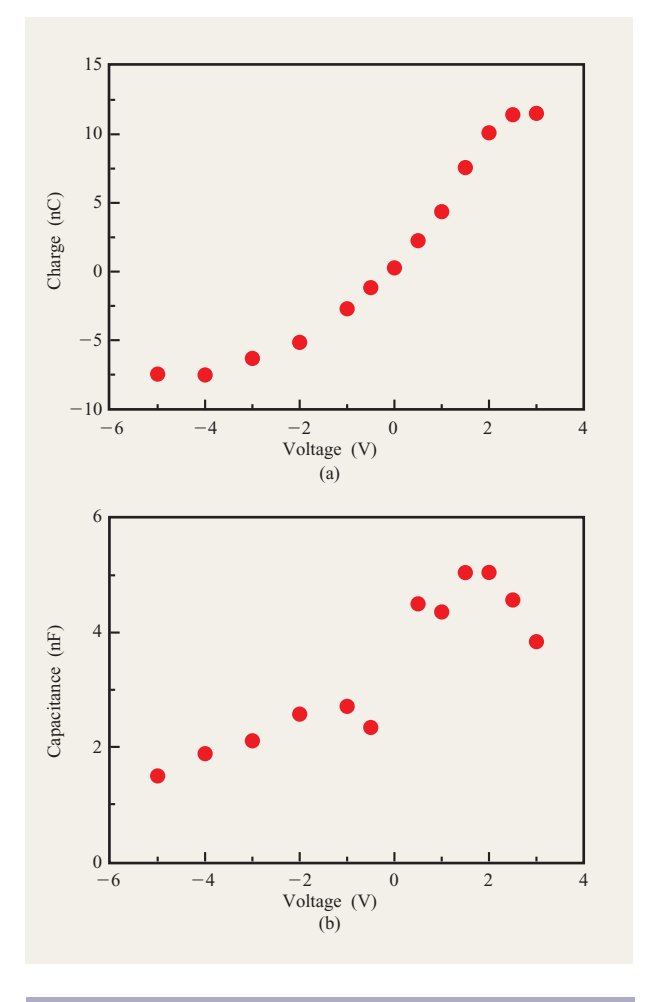


Figure 4

(a) Measured charge and (b) calculated capacitance of the same device as in Figure 2 after application of a different voltage for about 1 min. From [9].

and the first appearance of EL, an extrapolated rise time to reach a steady-state value, and finally the plateau value itself. The time-dependent behavior of the current is characterized by a fast initial decrease from a high starting point (the cutoff in Figure 5 is caused by the limited dynamic range of the oscilloscope) to the steady-state value, which corresponds to the current in the I-V characteristics at the given voltage. The initial decrease of the current also contains the charging current of the device. However, this process is expected to be much faster than the displayed decay, because with the given device capacitance of 2 nF and a series resistor of $100~\Omega$ (to measure the current), the resulting charging current should have decayed after roughly 5~RC time constants, yielding about $1~\mu s$ for this process.

The observation of delayed EL has been used to extract charge-carrier mobilities and their field dependence in

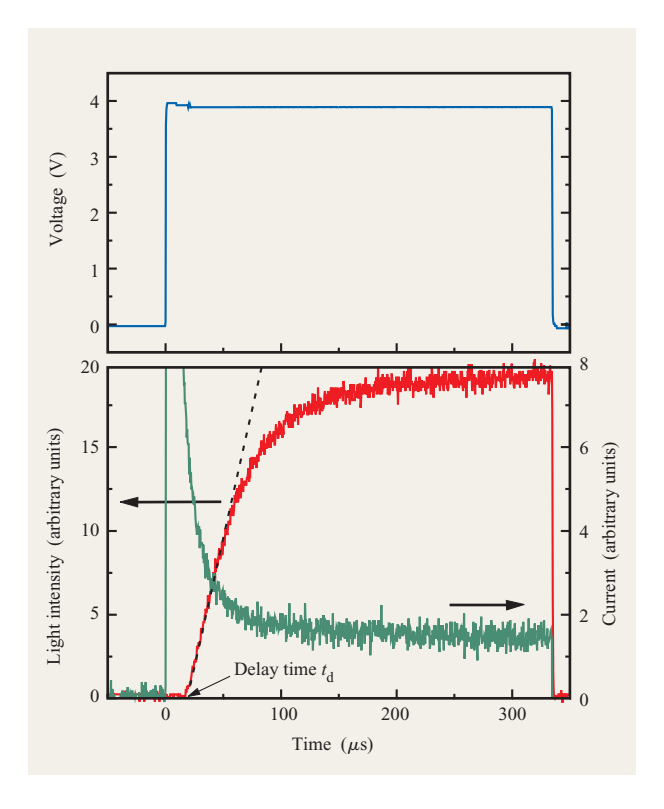


Figure 5

The upper graph shows a typical example of an applied rectangular voltage pulse. Below, the resulting response of light intensity and current of the OLED is depicted. The method used to determine the delay time is indicated. Adapted from [9].

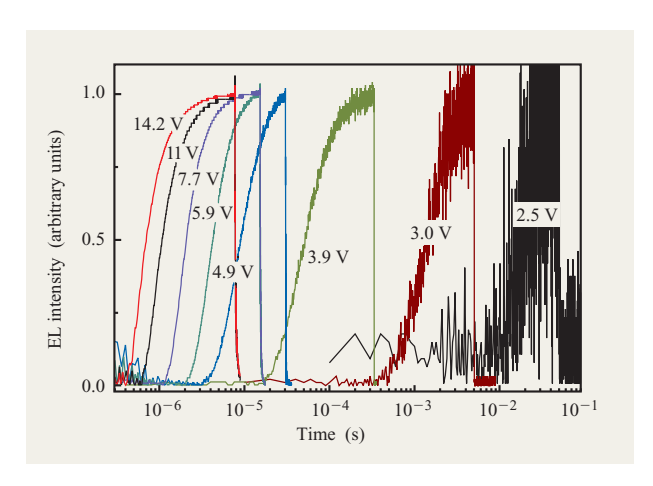


Figure 6

Normalized transient electroluminescence signals for an anode/CuPc (20 nm)/NPB (50 nm)/Alq $_3$ (65 nm)/Ca device for voltage pulses with different amplitudes and lengths. From [9].

polymeric and organic LEDs [16–20]. Additional information about the kinetics of charge-carrier recombination and trapping can be obtained from the rise to the steady state and the decay of the EL signal after the voltage pulse has been switched off. However, especially in multilayer structures, the interpretation of these transient experiments is not as straightforward as in a single-layer device because the injection of both types of carriers may not occur simultaneously [21].

Figure 6 shows normalized TEL traces for voltage pulses with different amplitudes and durations on a logarithmic time scale. The high sensitivity of the setup allows us to detect TEL with a reasonably good signal-tonoise ratio at a pulse amplitude as low as 2.5 V, which is only 0.4 V higher than the onset voltage detected in dc measurements. At this voltage the delay time is almost 10 ms. It rapidly becomes shorter with increasing pulse amplitude, and at a voltage of 5 V the delay time is only 3 µs, i.e., about three orders of magnitude lower. At 14.2 V (the highest voltage accessible with the pulse generator used), the delay time is less than 500 ns. Figure 7 shows the dependence on the applied voltage of the determined delay times as defined in Figure 5. Remarkably, the delay times vary over more than three orders of magnitude in a narrow voltage range between 2.5 and 5 V.

Figure 8 shows the transient response of the EL signal, and the inset shows the device current at a 5-V pulse amplitude on a logarithmic time scale extending from 1 μs to 300 ms. After reaching a first plateau value in the time range from about 40 to 400 μs , the EL signal and the current increase further—it takes more than 10 ms before they finally achieve a stationary value. The small bump in the EL signal at about 10 ms has no corresponding feature in the current. Detailed investigations have shown that this is an artifact of the photomultiplier system.

4. Discussion

Because electron-hole recombination in a multilayer device takes place at the interface between the hole-transporting and emitting layers, the NPB/Alq₃ interface is of crucial importance for device operation. To enhance device reliability and long-term stability, however, we inserted an additional CuPc hole-injecting/buffer layer. For the sake of simplicity we treat these devices as two-layer systems composed of a hole and an electron-conducting compartment having only one organic hetero-interface. Where necessary, we mention the peculiarities of the CuPc/NPB interface.

Steady-state device characteristics of organic lightemitting devices

From the *I–V* and EL–*V* characteristics shown in Figure 2, it is immediately obvious that the operating voltage range of the OLEDs investigated can be divided into two

regimes; in the forward bias regime V > 2 V, light emission is observed, and current flow is orders of magnitude higher than in the second regime, the region V < 2 V, where no light is emitted. The voltage in the forward direction, where the onset of significant current flow is detected, is commonly considered to be the built-in potential $V_{\rm BI}$, which is to a first approximation given by the difference between the work functions of the anode and cathode metals. In a system of one or more organic materials without free carriers sandwiched between two metal electrodes having different work functions, the external voltage must overcome the resulting built-in voltage before a net drift current can flow through the device. Therefore, the relevant quantity is not the applied voltage V but the corrected effective value $V - V_{\rm BI}$ [22]. For our experiment, we estimated a built-in potential V_{BI} of about 2 V by measuring the maximum open-circuit voltage of illuminated samples.

The observed dependence of the current on sweep speed and direction indicates that extremely slow processes are involved. Numerical simulations on NPB single-layer devices by Nguyen et al. show that the hysteresis observed in the *I–V* characteristics can qualitatively be explained by the presence of deep traps, which require large time constants to reach thermal equilibrium after a variation of the voltage across the device.²

A crucial point for a more quantitative understanding of the device characteristics is therefore the knowledge of the electric field distribution inside the individual layers. This is of overall importance because the hole-conducting (NPB) and electron-conducting materials (Alq₃) of this device show quite different charge-carrier transport properties. Whereas NPB and related triphenyl-amines are purely hole-conducting materials with relatively high hole mobilities and very weak dependence of the mobility on the electric field F [$\mu_{\rm h,NPB} = 6.1 \times 10^{-4} \ {\rm cm^2/Vs \cdot exp}$ (1.5 \times $10^{-3} \sqrt{\text{cm/V}} \cdot \sqrt{F}$], Alq₃ shows predominantly electron transport with lower carrier mobilities and a strong electric field dependence $[\mu_{e,Alq_2} = 7.1 \times 10^{-10} \text{ cm}^2/\text{Vs} \cdot$ $\exp{(1.2 \times 10^{-2} \sqrt{\text{cm/V}} \cdot \sqrt{F})}$ [23, 24]. On the other hand, recent time-of-flight and TEL measurements have shown that hole transport in Alq, cannot be neglected, although the low-field hole mobility is considerably lower than the electron mobility [$\mu_{h,Alq_3} = 6 \times 10^{-11} \text{ cm}^2/\text{Vs}$ · $\exp (9 \times 10^{-3} \sqrt{\text{cm/V}} \cdot \sqrt{F})$ [25, 26]. Owing to the strong field dependence of the charge-carrier mobility of holes and electrons in the Alq, layer, the time scale to reach a stationary charge distribution depends strongly on the electric field distribution in this layer. A further point concerns the injection of carriers from the electrodes into the organic and from one organic layer into the adjacent

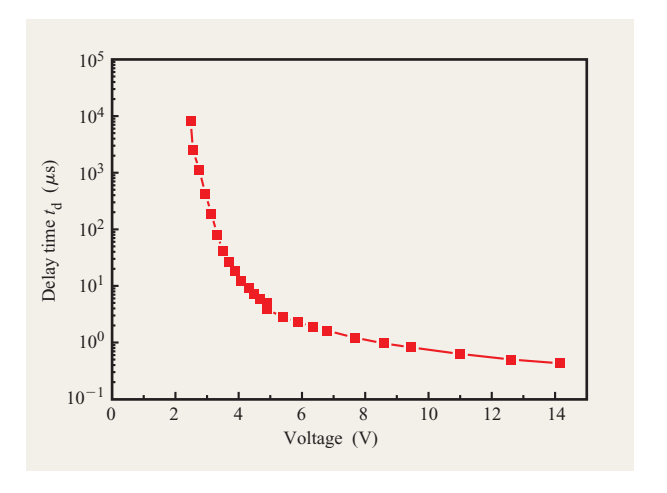


Figure 7

Delay time versus applied bias obtained from the transient electroluminescence signals shown in Figure 6.

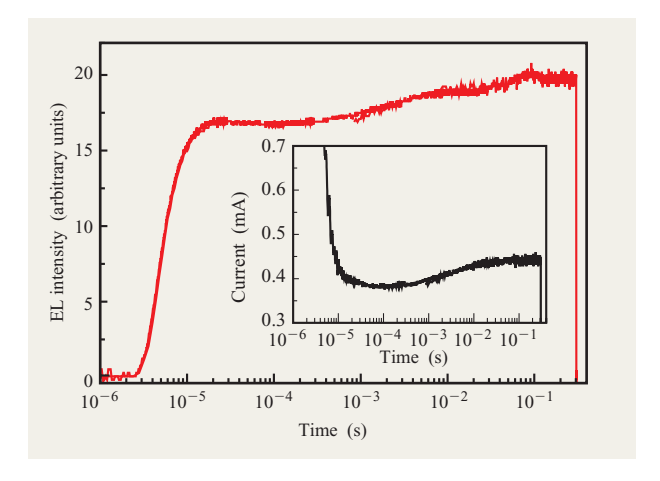


Figure 8

Transient electroluminescence at an amplitude of 5 V on a large time scale; the inset shows the corresponding current. For experimental reasons, the signal consists of five oscilloscope traces taken with different time scales.

one, where the electric field in the individual layers and at the interfaces also plays an important role.

To a first approximation, one can assume from the energy-level diagram of the OLED device shown in Figure 1 that the voltage drops homogeneously over the entire device. Since NPB and Alq₃ have similar dielectric constants, the electric field in the hole- and electron-conducting layers is given by $F^{(a)} = (V - V_{\rm BI})/d_{\rm tot}$, where $d_{\rm tot}$ is the total thickness of both organic layers. The

² P. H. Nguyen, S. Scheinert, S. Berleb, W. Brütting, and G. Paasch (preprint).

capacitance in this case would be $C^{(a)} = \varepsilon_r \varepsilon_0 A/d_{tot}$, where A is the device area and ε_{r} is the permittivity. However, such a situation is not very realistic for the OLED operated under forward bias conditions, because from the large difference in hole and electron mobility in NPB and Alq₃, respectively, one has to expect that the Alq₃ layer limits the current, where consequently most of the applied voltage will drop. Indeed, recent electroabsorption measurements by Rohlfing et al. have shown that the voltage drop at the Alq, layer for positive bias is almost ten times larger than that at the NPB layer [27]. Thus, the electric field in the NPB layer is to a first approximation negligible compared to the field in the Alq, layer; in the extreme example, $F_{\text{NPB}}^{(b)} = 0$, and in the Alq₃ layer, $F_{\rm Alq}^{(b)} = (V - V_{\rm BI})/d_{\rm Alq}^{(a)}$, which is larger than $F^{(a)}$. Such a discontinuity in the electric field must be accompanied by an accumulation of charge carriers at the interface (the simplest case being in an infinitely thin layer) via

$$\Delta F = \frac{\sigma}{\varepsilon_r \varepsilon_0},\tag{2}$$

where σ is the number of charges per unit area sitting at the interface, and equal dielectric constants ε_r in both materials have been assumed. The capacitance is now determined by the Alq₃ thickness alone and is, with $C^{(b)} = \varepsilon_r \varepsilon_0 A/d_{\text{Alg}^3}$, larger than $C^{(a)}$.

From our capacitance-voltage (C-V) measurements (Figure 3) we can indeed see that there is a transition from a situation similar to case (a), with the capacitance equal to the geometrical capacitance of the device for V < 0 V, to the situation in case (b) for V approaching 2 V, where the capacitance is now about twice as large as in the reverse bias direction. This corresponds well to the thickness of the Alq, layer of 65 nm compared to about 70 nm for the sum of the CuPc and NPB layer thicknesses. By a systematic variation of both organic layer thicknesses on ITO/NPB/Alq₃/Ca devices, Berleb et al. have recently found that the value of the capacitance in the reverse bias direction always corresponds to the total thicknesses of all organic layers, while the value at 2 V is determined solely by the thickness of the Alq₃ layer [28]. Moreover, the increase in the capacitance at a voltage well below the built-in voltage was explained by the presence of negative interfacial charges at the NPB/Alq, interface, resulting in a discontinuity of the electric field as discussed above. Our C-V measurements also prove that under a sufficiently large negative bias, the device actually behaves like a dielectric with no mobile charges inside the organic layers. The weak voltage dependence of the capacitance observed in this range can be attributed to the presence of the CuPc layer (presumably some residual doping) and is not seen if this layer is omitted. When the bias voltage is increased above 0 V, the capacitance

increases, indicating that the NPB layer has reached the flat-band condition, and its resistance drops drastically [28]. With increasing bias, holes are injected from the anode, gradually reducing immobile negative charges at the NPB/Alq₃ interface until at $V_{\rm BI}$ the negative interfacial charge is fully compensated and the device is in the flatband condition. The additional positive charges inside the device are directly measured in the discharge experiments shown in Figure 4. The crossover from the dielectric to the charged state of the device is observed at a voltage $V_{\rm c}$, which is given by the magnitude of the negative interfacial charges σ and the thickness of the Alq₃ layer via

$$\Delta F = \frac{V_{\rm c} - V_{\rm BI}}{d_{\rm Alq.}} = \frac{\sigma}{\varepsilon_{\rm c} \varepsilon_{\rm o}}.$$
 (3)

Using $V_{\rm c}\approx 0$ V, $V_{\rm BI}\approx 2$ V, and $\varepsilon_{\rm r}\approx 3.5$, the interfacial charge density can be estimated to be $\sigma\approx -5.9\times 10^{11}$ $e/{\rm cm}^2$, which is in good agreement with the value of $\sigma\approx -6.8\times 10^{11}$ $e/{\rm cm}^2$ obtained on ITO/NPB/Alq₃/Ca devices [28].

Transient response of organic light-emitting devices

The scenario described above has important consequences for the transient response of OLEDs, because the compensation of the negative interfacial charges cannot be expected a priori to occur instantaneously. This is directly seen in the frequency dependence of the capacitance, which shows that the enhanced capacitance between 0 and 2 V resulting from the redistribution of the electric field can only be monitored up to frequencies of ≈200 Hz. Furthermore, in the forward direction $(V > V_{\rm BI})$, the electric field inside the Alq3 layer and at the Alq3/cathode interface is enhanced by the presence of the positive space charge at the NPB/Alq, interface [29]. From this field enhancement at the cathode side, one must expect a strong influence on the electron-injecting properties of the cathode into Alq₃, even if the injection barrier is assumed to be small, as in the case of Ca as cathode.

Transferring the scenario described above to TEL experiments, several processes must occur following the application of a positive voltage pulse with $V > V_{\rm BI}$ before light emission can take place: injection of holes, compensation of negative charges, and buildup of positive space charge at the NPB/Alq, interface; injection of electrons at the cathode; and transport of electrons to the NPB/Alq₃ interface, where they can ultimately recombine radiatively with holes injected from NPB into Alq₃. Therefore, it is not as straightforward to obtain chargecarrier mobilities from the delayed onset of EL observed in a time-resolved EL experiment in these OLEDs, as has been reported for single-layer devices. The important question here is whether the observed delay times (as defined in Figure 5) originate from electron transport through the Alq, layer to the recombination zone, or from the buildup of the internal space charge and the concomitant redistribution of the electric field inside the device. A direct check whether the buildup of space charges contributes to the observed temporal response of the OLED can be obtained by superimposing a dc offset bias on the applied voltage pulse. Figure 9 compares two EL traces obtained with the same voltage amplitude of 4 V but different offset biases: 0 and 2 V. The bias value of 2 V is chosen just below the onset of double carrier injection in order to guarantee the compensation of negative charges at the NPB/Alq, interface, as has been proved by capacitance-voltage measurements. Figure 9 clearly shows that the delay times of the EL signal to a steady-state value are at least a factor of 2 shorter if a positive bias of 2 V is applied prior to the application of the 4-V voltage pulse; this directly proves that the buildup of space charge at the NPB/Alq, interface has a significant influence on the temporal response of light emission in this OLED structure. Also, the decay of the current to the steady state is much faster in the presence of the positive bias, which in turn shows that the initial high current and its temporal decay after the application of a voltage pulse are not given by the RC time constant of the setup, as discussed in Section 3. Instead, this temporal behavior of the current directly reflects the buildup of the internal space charge in the device. As the existence of positive space charge in the NPB layer reduces the electric field in the vicinity of the hole-injecting contact, the initial current at t = 0 in the absence of space charges is much higher than the steady-state current for $V > V_{\rm BI}$. By taking the integral of the current over time, one can directly estimate the accumulated charge injected into the device. The integration from t = 0 to 100 μ s yields a charge of 7.3 nC for zero offset bias and only 4.5 nC for 2 V positive bias. The difference of almost 3 nC is a crude estimate for the space charge built up by the positive bias of 2 V prior to the voltage pulse. This is in the same range as the values measured directly from the discharge experiments [Figure 4(a)].

Bearing in mind that the buildup of space charges has a non-negligible influence on TEL, one can nevertheless use the delay times obtained from the EL transients displayed in Figure 6 to calculate charge-carrier mobilities in Alq₃. In our device structure, EL first occurs when the leading charge carriers of each polarity meet in the Alq₃ layer close to the NPB/Alq₃ interface. At a given electrical field F and layer thickness d, the delay time t_d depends on the mobility μ as

$$t_{\rm d} = \frac{d}{\mu F} \,. \tag{4}$$

If the mobilities of both charge-carrier types in Alq₃ are very different, the higher drift mobility rather than the

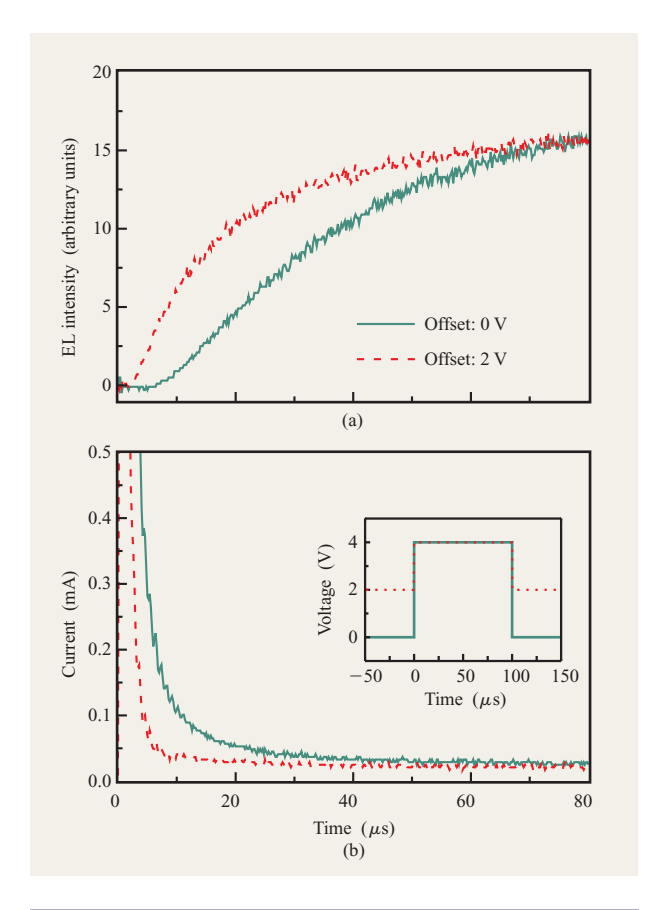


Figure 9

(a) Transient electroluminescence and (b) current at a pulse height of 4 V for two different offset bias values. The inset shows the applied rectangular voltage pulse for the two cases. Adapted from [9].

ambipolar mobility $\mu=\mu_{\rm h}+\mu_{\rm e}$ determines the delay time. From the delay time of the EL signal, one can calculate the mobility by taking into account the built-in voltage as

$$\mu = \frac{d}{t_{\perp}F} \quad \text{with} \quad F = \frac{V - V_{\text{BI}}}{d}. \tag{5}$$

Because the mobility of holes in NPB is approximately three orders of magnitude higher than that of electrons in Alq₃ ($\mu_{\rm h,NPB} \gg \mu_{\rm e,Alq_3}$) and because most of the applied voltage drops at the Alq₃ layer as discussed above, it is reasonable to consider only the thickness of the Alq₃ layer in the calculation of an electric field. Owing to the higher mobility of electrons compared to holes in Alq₃ ($\mu_{\rm e,Alq_3} \gg \mu_{\rm h,Alq_3}$), recombination takes place in the Alq₃ layer close to the NPB/Alq₃ interface; thus, the delay of EL is determined by the transit time of electrons in the Alq₃ layer [23, 25, 26].



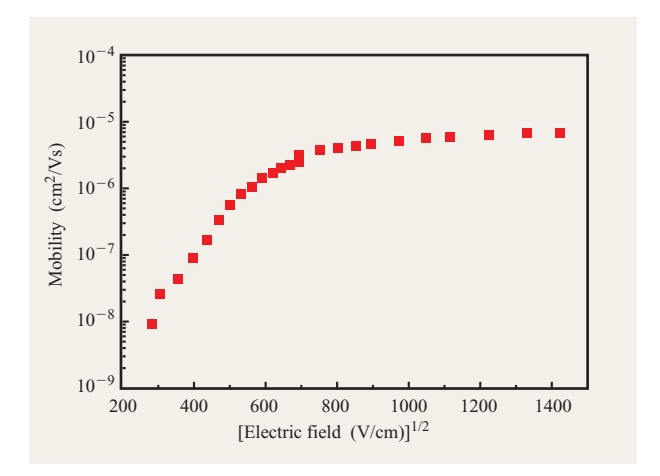


Figure 10

Calculated mobility values according to Equation (5) from the delay times displayed in Figure 7. A built-in voltage $V_{\rm BI}=2~{\rm V}$ was used to calculate the field.

Using the measured delay times (Figure 7), one can calculate a field-dependent electron mobility in Alq₃, as shown in Figure 10. A plot of the logarithm of the mobility vs. the square root of the electric field has been chosen because these amorphous materials are known to show a field-dependent mobility of the form $\mu \propto \exp(\beta \sqrt{F})$ [30], which is explained by a disorder formalism [31, 32] or the phenomenological Poole-Frenkel model [33]. In the logarithmic plot of the mobility versus \sqrt{F} (see Figure 10), two different slopes can be observed, with a crossover at about $\sqrt{F} = 700\sqrt{\text{V/cm}}$. In the low-field regime, a pronounced field dependence is observed, in which the calculated mobility seems to vary over more than two orders of magnitude; this is followed by the second regime, in which the determined mobility changes by only a factor of 2. This crossover between regions with different field dependences indicates that various processes are involved in the temporal EL response of these multilayer devices. In calculating the mobility from the experimental data, we have so far neglected the influence of the internal interface on the transient response. As discussed above, space charges build up with time at the NPB/Alq, interface, leading to an enhancement of the electric field in the Alq, layer and facilitating electron injection at the cathode. The time required for building up the space charge depends on the applied voltage pulse (i.e., the amount of current flow). Consequently, if the buildup of the internal space charge takes significantly longer than the transit of electrons through the Alq, layer, the delay time will be determined by the time required to build up the space charge and will then contain no information about the electron mobility in Alq₃. Therefore, we attribute the strong increase of the calculated mobility in the low-field region to a charging effect at internal interfaces rather than to a real field-dependent behavior of the mobility.

The control of the TEL response in heterolayer OLEDs by the buildup of an internal space charge inside the device has been observed experimentally and verified by numerical simulations on polymeric bilayer OLEDs by Nikitenko et al. [21]. They have shown that the temporal response (delay time of EL) depends very sensitively on the injection barriers of electrons and holes at the cathode and anode sides, respectively. For sufficiently large injection barriers, the buildup of the internal space charge can eventually fully control the transient response of the device.

Finally, we note that the delay time of the TEL signal does not contain all of the information about the timedependent response of these OLED devices. As seen in Figure 8 after a first plateau in the time range of some 10 to 100 µs has been reached, there is a further increase of EL and current on a much longer time scale up to about 10 ms. At present there is no definite explanation for the observed behavior. A possible origin could be dispersive transport of charge carriers leading to a spread of transit times over many orders of magnitude in time. However, if this is the dominant factor, one would expect to see a continuous rise of EL and current rather than the relatively distinct two steps observed. Probably the complex interplay among the buildup of the internal space charge, the concomitant redistribution of the electric field, and their feedback on charge-carrier injection and transport is responsible for this behavior. A possible shift or broadening of the recombination zone due to a nonnegligible hole mobility in Alq, [25, 26] may also contribute. Thus, further experiments coupled with numerical simulations are required in order to clarify the origin of the long-term response.

5. Conclusion

Our experimental results show that the electrical characteristics of organic light-emitting devices incorporating the hetero-interface between hole-conducting triphenyl-amine derivatives (e.g., NPB) and aluminum hydroxy-quinoline (Alq3) can be separated into three regimes. First, the built-in potential $V_{\rm BI}$ of approximately 2 V caused by the contact potential difference of the metal electrodes separates the voltage range into the forward bias regime ($V > V_{\rm BI}$), where double carrier injection, transport, and radiative recombination in the Alq3 layer close to the NPB interface occur. Second, for high reverse bias ($V \ll V_{\rm BI}$), the devices behave like a dielectric, with insulating material sandwiched between two metal electrodes. In particular, our capacitance–voltage measurements show that between

these two regimes there is a third regime between a critical value $V_{\rm c}$ depending on the Alq₃ thickness ($V_{\rm c}\approx 0~{\rm V}$ for a 65-nm-thick Alq₃ layer) and the built-in voltage. The observation of an enhanced device capacitance indicates the presence of negative interfacial charges at the NPB/Alq₃ interface, which are gradually compensated by injected holes as the built-in voltage is approached. The important consequences of this process are seen in the TEL response, which at low forward voltages is completely governed by the buildup of the internal space charge rather than by the transport of carriers through the Alq₃ layer.

Acknowledgments

The authors thank S. F. Alvarado, S. Barth, and S. Karg for valuable discussions, and M. Tschudy for preparing the substrates. W. B. acknowledges financial support from IBM Rüschlikon for hosting his visit.

References

- W. Helfrich and W. G. Schneider, "Recombination Radiation in Anthracene Crystals," *Phys. Rev. Lett.* 14, 229 (1965).
- C. W. Tang and S. A. Van Slyke, "Organic Electroluminescent Diodes," *Appl. Phys. Lett.* 51, 913–915 (1987).
- C. W. Tang, S. A. Van Slyke, and C. H. Chen, "Electroluminescence of Doped Organic Thin Films," *J. Appl. Phys.* 65, 3610–3616 (1989).
- M. A. Lampert and P. Mark, Current Injection in Solids, Academic Press, Inc., New York, 1970.
- C. Giebeler, H. Antoniadis, D. D. C. Bradley, and Y. Shirota, "Influence of the Hole Transport Layer on the Performance of Organic Light-Emitting Diodes," *J. Appl. Phys.* 85, 608–615 (1999).
- S. Berleb, W. Brütting, M. Schwoerer, R. Wehrmann, and A. Elschner, "Effect of Majority Carrier Space Charges on Minority Carrier Injection in Dye Doped Polymer Light-Emitting Devices," J. Appl. Phys. 83, 4403–4409 (1998).
- P. W. M. Blom, M. J. de Jong, and J. J. M. Vleggaar, "Electron and Hole Transport in Poly(p-phenylene Vinylene) Devices," *Appl. Phys. Lett.* 68, 3308–3310 (1996).
- L. Bozano, S. A. Carter, J. C. Scott, G. G. Malliaras, and P. J. Brock, "Temperature- and Field-Dependent Electron and Hole Mobilities in Polymer Light-Emitting Diodes," *Appl. Phys. Lett.* 74, 1132–1134 (1999).
- W. Brütting, H. Riel, T. Beierlein, and W. Riess, "Influence of Trapped and Interfacial Charges in Organic Multilayer Light-Emitting Devices," J. Appl. Phys. (in press).
- J. Kanicki, in *Handbook of Conducting Polymers*, T. A. Skotheim, Ed., Marcel Dekker, New York, 1986, Ch. 17.
- D. M. Taylor, H. Gomes, A. E. Underhill, S. Edge, and P. I. Clemenson, "Effect of Oxygen on the Electrical Characteristics of Field Effect Transistors Formed from Electrochemically Deposited Films of Poly(3-methylthiophene)," J. Phys. D: Appl. Phys. 24, 2032–2038 (1991).
- M. Meier, S. Karg, and W. Riess, "Light-Emitting Diodes Based on Poly-p-phenylene-vinylene: II. Impedance Spectroscopy," *J. Appl. Phys.* 82, 1961–1966 (1997).
- J. Scherbel, P. H. Nguyen, G. Paasch, W. Brütting, and M. Schwoerer, "Temperature Dependent Broadband

- Impedance Spectroscopy on Poly-(p-phenylene-vinylene) Light-Emitting Diodes," J. Appl. Phys. 83, 5045–5055 (1998).
- 14. A. K. Hassan and R. D. Gould, "The Effects of Exposure to Oxygen and Annealing on the Conductivity of Copper Phthalocyanine Thin Films," *J. Phys.: Condens. Matter* 1, 6679–6684 (1989).
- H. Riel, "Ladungsträgerinjektion, Transport und Rekombination in organischen LEDs: Von Einschiebestrukturen zu effizienten blauen OLEDs," Diplomarbeit, Universität Erlangen, Germany, 1998.
- C. Hosokawa, H. Tokailin, H. Higashi, and T. Kusumoto, "Transient Behavior of Organic Thin Film Electroluminescence," *Appl. Phys. Lett.* 60, 1220–1222 (1992).
- H. Vestweber, J. Oberski, A. Greiner, W. Heitz, R. F. Mahrt, and H. Bässler, "Electroluminescence from Phenylenevinylene-Based Polymer Blends," *Adv. Mater. Opt. Electron.* 2, 197–204 (1993).
- S. Karg, V. Dyakonov, M. Meier, W. Riess, and G. Paasch, "Transient Electroluminescence of PPV LEDs," Synth. Met. 67, 165-168 (1994).
- H. Nakamura, C. Hosokawa, and T. Kusumoto, "Transient Behavior of Organic EL Cells," in *Inorganic and Organic Electroluminescence*, R. H. Mauch and H.-E. Gumlich, Eds., Wissenschaft & Technik Verlag, Berlin, 1996, pp. 95–100.
- S. Barth, P. Müller, H. Riel, P. F. Seidler, W. Riess, H. Vestweber, and H. Bässler, "Electron Mobility in Alq₃ Determined via Transient Electroluminescence from Single- and Multilayer Organic Light-Emitting Diodes," J. Appl. Phys., in press.
- V. R. Nikitenko, Y.-H. Tak, and H. Bässler, "Rise Time of Electroluminescence from Bilayer Light-Emitting Diodes," J. Appl. Phys. 84, 2334–2340 (1998).
- 22. J. C. Scott, S. Karg, and S. A. Carter, "Bipolar Charge and Current Distributions in Organic Light-Emitting Diodes," *J. Appl. Phys.* **82**, 1454–1460 (1997).
- R. G. Kepler, P. M. Beeson, S. J. Jacobs, R. A. Anderson, M. B. Sinclair, V. S. Valencia, and P. A. Cahill, "Electron and Hole Mobility in Tris(8-hydroxyquinolinolato-N1,O8) Aluminum," *Appl. Phys. Lett.* 66, 3618–3620 (1995).
- T. Tsutsui, H. Tokuhisa, and M. Era, "Charge Carrier Mobilities in Molecular Materials for Electroluminescent Diodes," in *Polymer Photonic Devices, Proc. SPIE* 3281, 230–239 (1998).
- A. G. Mückl, S. Berleb, W. Brütting, and M. Schwoerer, "Transient Electroluminescence Measurements on Organic Hetero Layer Light Emitting Diodes," *Synth. Met.* 111–112, 91–94 (2000).
- S. Naka, H. Okada, H. Onnagawa, J. Kido, and T. Tsutsui, "Time-of-Flight Measurement of Hole Mobility in Aluminum(III) Complexes," *Jpn. J. Appl. Phys.* 38, L-1252–L-1254 (1999).
- F. Rohlfing, T. Yamada, and T. Tsutsui, "Electroabsorption Spectroscopy on Tris-(8-hydroxyquinoline) Aluminum-Based Light-Emitting Diodes," J. Appl. Phys. 86, 4978–4984 (1999).
- 28. S. Berleb, W. Brütting, and G. Paasch, "Interfacial Charges and Electric Field Distribution in Organic Hetero-Layer Light-Emitting Devices," *Organic Electron.* 1, 41–47 (2000).
- 29. M. Matsamura, A. Ito, and Y. Miyamae, "Accumulation of Positive Charges in Organic Light-Emitting Diodes with a Double-Layer Structure," *Appl. Phys. Lett.* **75**, 1042–1044 (1999).
- P. M. Borsenberger and D. S. Weiss, Organic Photoreceptors for Imaging Systems, Marcel Dekker, New York, 1993.
- H. Bässler, "Charge Transport in Disordered Organic Photoconductors," Phys. Stat. Sol. B 175, 15 (1993).
- 32. D. H. Dunlap, P. E. Parris, and V. M. Kenkre, "Charge-Dipole Model for the Universal Field Dependence of

- Mobilities in Molecularly Doped Polymers," *Phys. Rev. Lett.* **77**, 542–545 (1996).
- W. D. Gill, "Drift Mobilities in Amorphous Charge-Transfer Complexes of Trinitrofluorenone and Polynvinylcarbazole," J. Appl. Phys. 43, 5033–5040 (1972).

Received May 21, 2000; accepted for publication September 25, 2000

Walter Riess IBM Research, Zurich Research Laboratory, 8803 Rüschlikon, Switzerland (wri@zurich.ibm.com). Dr. Riess received a degree in physics (Dipl. Phys.) from the University of Bayreuth, Germany, in 1987. In 1991, he received a Ph.D. degree from the University of Bayreuth for his thesis on nonlinear conduction phenomena in organic charge density wave conductors. From 1992 to 1995, he was a research assistant in the Physical Institute of the University of Bayreuth, where he investigated charge-carrier injection, transport, and recombination processes in organic lightemitting diodes. During his stay as a visiting scientist at the IBM Zurich Research Laboratory in 1994, he initiated a project on organic light-emitting diodes and, in October 1995, he joined the IBM Zurich Research Laboratory as a Research Staff Member in the Display Technology group. Dr. Riess finished his habilitation in 1996 with a thesis on polymeric light-emitting diodes. In October 1998, he became manager of the Display Technology group and continues to focus on display applications of electroluminescent organic materials.

Heike Riel IBM Research, Zurich Research Laboratory, 8803 Rüschlikon, Switzerland (hei@zurich.ibm.com). Mrs. Riel studied physics at the University of Erlangen-Nuremberg, Germany. In 1996, she pursued practical training at the Institute of Technical Physics in Erlangen, working on the optical characterization of GaAs/AlGaAs heterostructures. In August 1996 she began a four-month internship at the Hewlett-Packard Research Laboratory, Palo Alto, working on the incorporation of metal/semiconductor/metal photodetector arrays with microlens arrays. In April 1997 she joined the Display Technology group at the IBM Zurich Research Laboratory to conduct her master's thesis work, focusing on the injection, transport, and recombination processes of charge carriers in organic light-emitting devices. In August 1998 she received a degree in physics (Dipl. Phys. Univ.) from the University of Erlangen-Nuremberg. Since then, she has been pursuing work on her Ph.D. thesis on organic electroluminescent devices for display applications within the Display Technology group at the IBM Zurich Research Laboratory.

Tilman Beierlein IBM Research, Zurich Research Laboratory, 8803 Rüschlikon, Switzerland (tib@zurich.ibm.com). Mr. Beierlein studied electrical engineering at the University of Ulm, Germany. After receiving an undergraduate degree, he was with the Optoelectronics Department of the University of Ulm, where he pursued work on photoassisted wet chemical etching of gallium nitride. In October 1996 he began a six-month internship in the Display Technology group of the IBM Zurich Research Laboratory. In August 1997 he rejoined the IBM Zurich Research Laboratory to perform his master's thesis on the fabrication and characterization of thin InGaN films for application in organic light-emitting devices. In February 1998 he received a degree in electrical engineering (Dipl. Ing.) from the Optoelectronics Department of the University of Ulm. Since mid-1998 he has been working on

his Ph.D. thesis in the Display Technology group of the IBM Zurich Research Laboratory on research and technology of organic electroluminescent devices for display applications.

Wolfgang Brütting *Experimental Physics II*, University of Bayreuth, 95440 Bayreuth, Germany (wolfgang.bruetting@uni-bayreuth.de). Dr. Brütting studied physics at the Universities of Erlangen-Nuremberg and Bayreuth, Germany, graduating in 1992. He received a Ph.D. degree from the University of Bayreuth in 1995 for his thesis on charge transport in quasi-one-dimensional charge density wave systems. Since then, he has been a research assistant in experimental physics at the University of Bayreuth, where he heads the organic semiconductors group. Dr. Brütting has been a visiting scientist at Kyushu University, Japan, and at the IBM Zurich Research Laboratory. His current research interests include charge transport in organic semiconductor devices, especially light-emitting diodes from conjugated polymers and low-molecular-weight materials.

Peter Müller IBM Research, Zurich Research Laboratory, 8803 Rüschlikon, Switzerland (pmu@zurich.ibm.com). Mr. Müller is a Research Staff Member at the IBM Zurich Research Laboratory. He is currently involved in the OLED project, where his main interests are electrified interfaces. He joined IBM in 1987 after having received a degree in computer science from the Brugg-Windisch Polytechnical Institute in Switzerland. From 1994 to 1996, he was a guest scientist at the Exploratory Research and Technology Organization (ERATO) at Tohoku University, Japan.

Paul F. Seidler IBM Research, Zurich Research Laboratory, 8803 Rüschlikon, Switzerland (pfs@zurich.ibm.com). Dr. Seidler is manager of Science and Technology at the IBM Zurich Research Laboratory. His department pursues research in the fields of micromechanics, molecular-scale engineering, display technology, optical communications, advanced materials processing and characterization, and computational materials science. Dr. Seidler received a B.S. degree in chemistry from the California Institute of Technology in 1980 and a Ph.D. degree in chemistry from the University of California at Berkeley in 1985 for his thesis in the field of mechanistic organometallic chemistry. After a postdoctoral fellowship at Exxon Corporate Research, he joined the IBM Thomas J. Watson Research Center, where he worked on a variety of scientific studies related to semiconductor processing technology, in particular the kinetics and mechanisms of metal chemical vapor deposition. After serving a year as Technical Assistant to the Vice President, Systems, Technology and Science for the IBM Research Division, he moved to the Zurich Research Laboratory to become head of the Display Technology group and IBM's organic lightemitting diode project.